Cyclic nucleotide phosphodiesterase 1C contributes to abdominal aortic aneurysm

Chongyang Zhang[a,b,1], Hongmei Zhao[c,1], Yujun Cai[a], Jian Xiong[a,c], Amy Mohan[a], Danfei Lou[a,2], Hangchuan Shi[d,e], Yishuai Zhang[a], Xiaochun Long[f], Jing Wang[c,3], and Chen Yan[a,3]

[a]Aab Cardiovascular Research Institute, School of Medicine and Dentistry, University of Rochester, Rochester, NY 14642; [b]Department of Pharmacology and Physiology, School of Medicine and Dentistry, University of Rochester, Rochester, NY 14642; [c]State Key Laboratory of Medical Molecular Biology, Department of Pathophysiology, Institute of Basic Medical Sciences, Chinese Academy of Medical Sciences, Peking Union Medical College, Beijing 100730, China; [d]Department of Clinical and Translational Research, University of Rochester Medical Center, Rochester, NY 14642; [e]Department of Public Health Sciences, University of Rochester Medical Center, Rochester, NY 14642; and [f]Vascular Biology Center, Medical College of Georgia at Augusta University, Augusta, GA 30912

Edited by Barry S. Coller, The Rockefeller University, New York, NY, and approved May 25, 2021 (received for review May 2, 2021)

Abdominal aortic aneurysm (AAA) is characterized by aorta dilation due to wall degeneration, which mostly occurs in elderly males. Vascular aging is implicated in degenerative vascular pathologies, including AAA. Cyclic nucleotide phosphodiesterases, by hydrolyzing cyclic nucleotides, play critical roles in regulating vascular structure remodeling and function. Cyclic nucleotide phosphodiesterase 1C (PDE1C) expression is induced in dedifferentiated and aging vascular smooth muscle cells (SMCs), while little is known about the role of PDE1C in aneurysm. We observed that PDE1C was not expressed in normal aorta but highly induced in SMC-like cells in human and murine AAA. In mouse AAA models induced by Angiotensin II or periaortic elastase, PDE1C deficiency significantly decreased AAA incidence, aortic dilation, and elastin degradation, which supported a causative role of PDE1C in AAA development in vivo. Pharmacological inhibition of PDE1C also significantly suppressed preestablished AAA. We showed that PDE1C depletion antagonized SMC senescence in vitro and/or in vivo, as assessed by multiple senescence biomarkers, including senescence-associated β-galactosidase activity, γ-H2AX foci number, and p21 protein level. Interestingly, the role of PDE1C in SMC senescence in vitro and in vivo was dependent on Sirtuin 1 (SIRT1). Mechanistic studies further showed that cAMP derived from PDE1C inhibition stimulated SIRT1 activation, likely through a direct interaction between cAMP and SIRT1, which leads to subsequent up-regulation of SIRT1 expression. Our findings provide evidence that PDE1C elevation links SMC senescence to AAA development in both experimental animal models and human AAA, suggesting therapeutical significance of PDE1C as a potential target against aortic aneurysms.

abdominal aortic aneurysm | vascular smooth muscle cell | phosphodiesterase | senescence

Aortic wall is subjected to continuous and high hemodynamic stress. The normal contractile function of smooth muscle cells (SMCs) and their ability to synthesize extracellular matrix (ECM), especially elastic fibers, are key for aorta to maintain structure integrity and withstand hemodynamic stress. SMC loss and matrix degradation predispose aorta to dilation and rupture in aneurysmal diseases. The most common form of aortic aneurysm (AA) is abdominal AA (AAA) that mainly occurs in elderly male (1). The rupture of aneurysm has high mortality and requires immediate surgical repair. The current challenge is the lack of effective therapeutics to prevent aneurysm progression and rupture (1). SMC phenotypic modulation under pathological circumstances, frequently referred to as "synthetic" or myofibroblast-like phenotype change, are associated with aberrant cellular properties and implicated in aneurysm development (2). Increasing experimental evidence suggest that cellular senescence is associated with accelerated vascular aging, such as atherosclerosis and AA (3). For example, cultured SMCs from human AAA showed increased telomere attrition and DNA double strand breaks (4), diminished proliferative capacity, and limited life span (5). Nicotinamide phosphoribosyltransferase–dependent nicotinamide adenine dinucleotide (NAD^+) fueling system protects against media degeneration, which is associated with decreased SMC senescence and DNA damage (6). Age-associated reduction of Sirtuin 1 (SIRT1) expression in SMC drive medial layers senescence and predisposes aorta to angiotensin II (Ang II)–induced AAA in mice (7). These findings highlight the role of SMC senescent phenotype in aneurysm.

Cyclic nucleotides, cAMP and cGMP, are important in regulating smooth muscle contractile function and maintaining vascular wall structural integrity. The degradation of cAMP and cGMP is catalyzed by a large family of PDEs with more than 100 different PDE variants derived from 21 genes and grouped into 11 broad families (PDE1 to PDE11) (8). PDEs are expressed in a cell/tissue-specific manner, and alterations of PDE expression/activation have been implicated in various diseases (8). Increasing evidence has

Significance

The rupture of abdominal aortic aneurysm (AAA) has high mortality while lacking effective therapeutics to prevent aneurysm progression. Identifying the regulators underlying aneurysm pathogenesis is essential. Herein, we reported induction of PDE1C in smooth muscle cell (SMC)–like cells of human and mouse AAA. Using genetic approaches, we demonstrated a causative role of cyclic nucleotide phosphodiesterase 1C (PDE1C) in experimentally induced AAA. More importantly, we revealed that pharmacological PDE1 inhibition attenuated the progression of preestablished AAA. Mechanistically, PDE1C-controlled cAMP suppresses SMC senescence and AAA development through cAMP-mediated direct interaction and activation of SIRT1. Given that PDE1 inhibitors have been proposed in clinical trials, our findings may have high therapeutic significance for the potential of using PDE1 inhibitors in treating AAA.

Author contributions: C.Z., H.Z., Y.C., X.L., J.W., and C.Y. designed research; C.Z., H.Z., Y.C., J.X., A.M., D.L., and Y.Z. performed research; C.Z. and X.L. contributed new reagents/analytic tools; C.Z., H.Z., Y.C., J.X., A.M., D.L., and H.S. analyzed data; and C.Z. and C.Y. wrote the paper.

The authors declare no competing interest.

This article is a PNAS Direct Submission.

[1]C.Z. and H.Z. contributed equally to this work.

[2]Present address: Department of Geriatrics, Shanghai Municipal Hospital of Traditional Chinese Medicine, Shanghai University of Traditional Chinese Medicine, Shanghai 200071, China.

[3]To whom correspondence may be addressed. Email: Chen_Yan@URMC.Rochester.edu and wangjing@ibms.pumc.edu.cn.

This article contains supporting information online at https://www.pnas.org/lookup/suppl/doi:10.1073/pnas.2107898118/-/DCSupplemental.

Published July 26, 2021.

indicated that there are multiple spatially discrete and functionally distinct cAMP/cGMP nanodomains and signalosomes in each cell, which are associated with distinct compartmentalized multiprotein complexes composing different receptors, cyclases, and PDEs (8). A few literature reports have suggested the potential links of cAMP/cGMP signaling with aneurysms. For example, SMC-specific ablation of $G_{s\alpha}$, a G protein responsible for cAMP production, exaggerated AAA in mice (9). In contrast, a recent study reported that a gain-of-function mutation in human cGMP-dependent protein kinase 1 (PKG1) plays a causative role in thoracic aortic aneurysm and aortic dissection (10). These results suggest that the stimulation of cAMP or cGMP signaling may have different or even opposite effects in AA/dissections. Different PDEs may regulate different cAMP and/or cGMP nanodomains and mediate distinct cellular functions. The functions of different PDE-regulated cyclic nucleotide signaling in AA are poorly understood, which is of great significance to be investigated, given many PDE inhibitors are under clinical uses or trials for treating various diseases.

PDE1C is a Ca^{2+}/calmodulin-stimulated enzyme and hydrolyzes both cAMP and cGMP with high affinities in the cell-free system (8). We and others have previously shown that PDE1C expression is selectively induced in dedifferentiated vascular

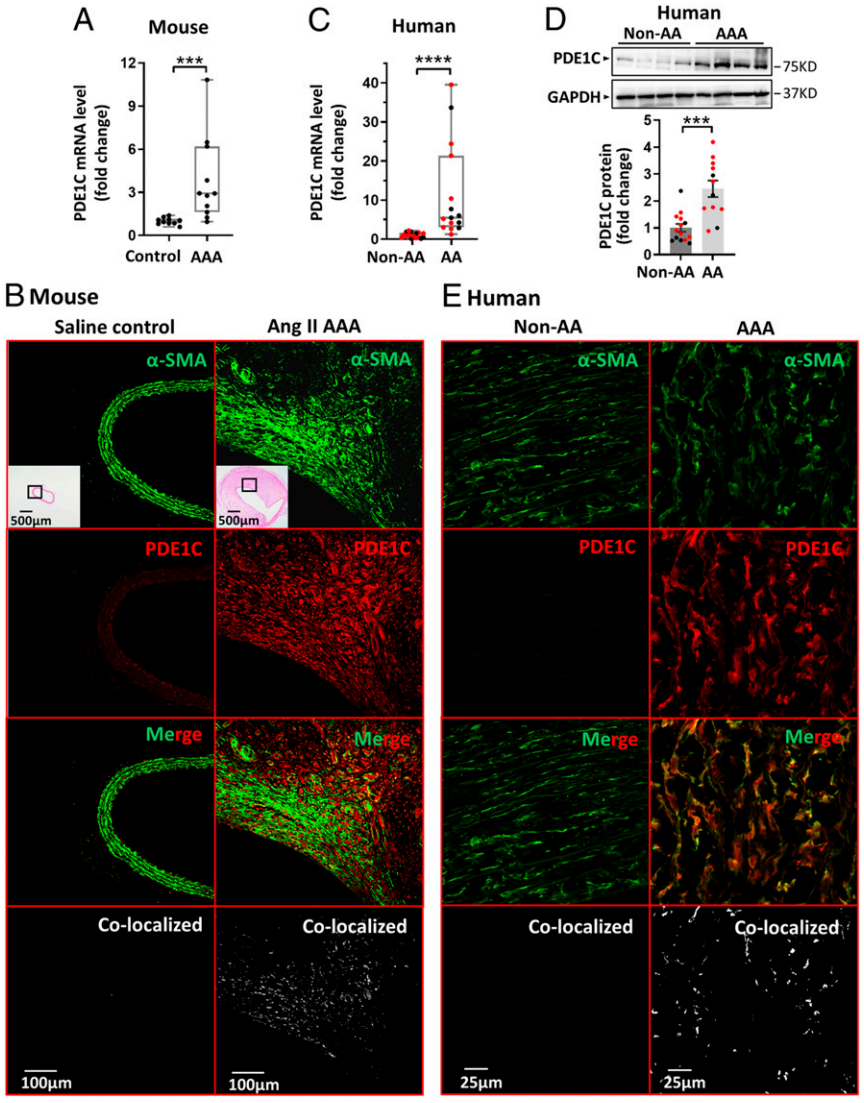

Fig. 1. PDE1C expression is induced in mouse and human AAA. (*A* and *B*) ApoE$^{-/-}$ male mice were infused with Ang II (1.4 mg/kg/d) through mini pumps for 28 d or saline as controls. (*A*) PDE1C mRNA levels in abdominal aortas from control or AAA by qPCR normalized to GAPDH. ***$P < 0.001$, Mann–Whitney *U* test, and median with interquartile range. For controls, $n = 10$, and for AAA, $n = 11$. (*B*) Representative immunostaining of PDE1C and α-SMA (SMC marker) in mouse cross-sections of suprarenal abdominal aortas from control or AAA. Bottom panels are the colocalized signal of PDE1C and α-SMA through colocalization analysis. At least three sets of different tissue samples were performed in separate experiments with similar observations. (*C*–*E*) Human AAA samples (red dots) and aneurysms at other aortic locations (black dots) were used as AA. Human nonaneurysmal aorta at abdominal (red dots) and at other aortic locations (black dots) were used as controls. (*C*) PDE1C mRNA levels measured by qPCR, normalized to GAPDH. $P = 0.0002$ abdominal controls versus AAA, Mann–Whitney *U* test, abdominal controls ($n = 10$), and AAA ($n = 9$). ****$P < 0.0001$ controls versus AA, Mann–Whitney *U* test, median with interquartile range, controls ($n = 16$), and AA ($n = 15$). (*D*) PDE1C protein levels by WB. $P = 0.002$ abdominal controls versus AAA, unpaired Student's *t* test, abdominal controls ($n = 8$), and AAA ($n = 9$). ***$P < 0.001$ controls versus AA, unpaired Student's *t* test, mean ± SEM, controls ($n = 14$), and AA ($n = 12$). Upper representative blots are human nonaneurysmal abdominal aorta and human AAA samples. (*E*) Representative immunostaining of PDE1C and α-SMA in cross-sections of human nonaneurysmal abdominal aorta or human AAA. Bottom panels are the colocalized signal of PDE1C and α-SMA by colocalization analysis. At least three different sets of human samples were performed in separate experiments with similar observations.

SMC from different species and vessel beds but not in the normal contractile SMCs (11, 12) nor in endothelial cells (ECs) (13). Cultured senescent human vascular SMCs have also been reported to have increased PDE1C expression (14). Therefore, it is of great interest to determine the role and underlying mechanism of PDE1C in AAA development. In this study, we evaluated the up-regulation of PDE1C in human and mouse AAA tissues. Using genetically engineered PDE1C knockout (KO) mice and pharmacological PDE1 inhibitor, we determined a causative role of PDE1C in vascular pathogenesis and AAA development, as well as tested the pharmacological effect of PDE1 inhibitor on intervening preestablished AAA progression. Moreover, we established a mechanism by which PDE1C stimulates vascular SMC senescence via attenuating cAMP and SIRT1 activation, which at least partially contributes to PDE1C regulation of AAA development.

Results

PDE1C Expression Is Induced in Mouse and Human AAA. We first examined PDE1C expression in mouse AAA lesions. Mouse AAA was induced by chronic infusion of Ang II for 28 d in ApoE$^{-/-}$ male mice (15). We found that PDE1C messenger RNA (mRNA) was up-regulated in AAA, compared to control samples from saline-infused mice (Fig. 1*A*). We also performed double immunostaining of PDE1C and smooth muscle α-actin (α-SMA), a marker for both differentiated contractile and dedifferentiated synthetic SMCs (or myofibroblasts) (Fig. 1*B* and *SI Appendix*, Fig. S1 show more examples). The results showed that PDE1C staining was neglectable in the control aortas as anticipated. PDE1C staining was observed prominently, although not exclusively, in α-SMA–positive cells in AAA lesions, suggesting that PDE1C expression can be induced in synthetic SMC-like cells.

We also examined PDE1C mRNA and protein levels in human AA tissues (Fig. 1 *C* and *D*). Aneurysmal aortas were collected during surgical repair at AAA (Fig. 1 *C* and *D*, red dots) or other aortic locations (Fig. 1 *C* and *D*, black dots). Age-matched nonaneurysmal aorta samples were collected at abdominal (Fig. 1 *C* and *D*, red dots) or other aortic locations (Fig. 1 *C* and *D*, black dots) from coronary artery bypass surgery, kidney artery bypass surgery, or organ donors. The human sample information is included in *SI Appendix*, Table S1. PDE1C expression was significantly elevated in human AAA versus abdominal aortic controls, as well as AA versus aortic controls, at both mRNA (Fig. 1*C*) and protein levels (Fig. 1*D*). PDE1C expression levels appear to be similar among AAA and AA from other parts of aorta. Immunofluorescent staining on human sections revealed a similar induction of PDE1C expression in SMC-like cells of AAA wall (Fig. 1*E*). PDE1C antibody specificity was supported by negative controls performed in mouse and human AAA sections (*SI Appendix*, Fig. S2 *A* and *C*) and in AAA of PDE1C$^{-/-}$ApoE$^{-/-}$ mice (*SI Appendix*, Fig. S2*B*). These data suggest that PDE1C expression was induced largely in SMC-like cells in human and mouse AAA lesions.

PDE1C Deficiency Alleviates Ang II–Induced AAA Formation in ApoE$^{-/-}$ Mice. To determine the role of PDE1C in AAA formation, we first evaluated the effect of PDE1C deficiency on AAA development using global PDE1C KO (PDE1C$^{-/-}$) mice under the ApoE$^{-/-}$ background in the Ang II infusion model. This widely used Ang II model recapitulates many aspects of AAAs, including luminal dilation, medial degeneration, and aneurysm rupture (15). PDE1C$^{-/-}$ApoE$^{-/-}$ mice have normal feeding/mating behaviors. The 12-wk-old PDE1C$^{-/-}$ApoE$^{-/-}$ male mice and control PDE1C wild-type male mice (PDE1C$^{+/+}$ApoE$^{-/-}$) were infused with Ang II (1,000 ng/kg/min) via mini pumps for 28 d. Ang II infusion increased blood pressure similarly in PDE1C$^{+/+}$ApoE$^{-/-}$ and PDE1C$^{-/-}$ApoE$^{-/-}$ mice (*SI Appendix*, Fig. S3), indicating that PDE1C does not regulate blood pressure. This is consistent with the fact that PDE1C is not expressed in contractile SMCs of normal vessels (11). No AAA was found in saline-infused mice (Fig. 2*A*). AAA is defined as a 50% or greater increase of abdominal aorta maximal width compared to normal (7). In Ang II–infused groups, AAA incidence in PDE1C$^{+/+}$ApoE$^{-/-}$ mice was 80.95% (17 out of 21), much higher than the 40.0% (8 out of 20) observed in PDE1C$^{-/-}$ApoE$^{-/-}$ mice (Fig. 2*B*). Ang II infusion caused a greater increase in the maximal abdominal aortic diameter in PDE1C$^{+/+}$ApoE$^{-/-}$ mice compared to PDE1C$^{-/-}$ApoE$^{-/-}$ mice (Fig. 2*C*). *SI Appendix*, Fig. S4 includes images of all AAA samples shown in Fig. 2 *B* and *C*. Approximately 35.72% of PDE1C$^{+/+}$ApoE$^{-/-}$ mice died from aortic dissection or rupture, but none of the PDE1C$^{-/-}$ApoE$^{-/-}$ mice died by the end of 4-wk Ang II infusion (Fig. 2*D*). This was accompanied with more severe elastin degradation in AAA of PDE1C$^{+/+}$ApoE$^{-/-}$ mice, depicted by breaks and fiber thinning via Van Gieson elastin (VVG) staining (Fig. 2*E*). Semi-quantitative analysis of the elastin degradation score used a previously defined arbitrary scale from 1 to 4, with 1 representing no visible disruption of medial elastin lamellae and 4 representing a severe transmural elastin break (Fig. 2*F* and *SI Appendix*, Fig. S5)

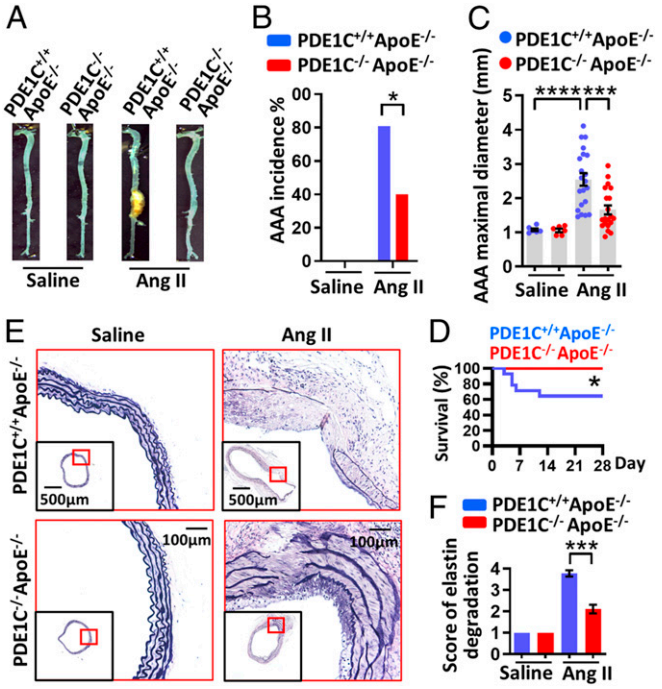

Fig. 2. PDE1C deficiency alleviates Ang II–induced AAA formation in ApoE$^{-/-}$ mice. The 12-wk-old male PDE1C$^{+/+}$ApoE$^{-/-}$ and PDE1C$^{-/-}$ApoE$^{-/-}$ mice were infused with Ang II (to induce AAA) or saline (as controls). (*A*) Representative images of mice aorta in each group. (*B*) AAA incidence (defined as ≥50% than control abdominal aorta external width). *$P < 0.05$ by Fisher's exact test. (*C*) AAA maximal diameter of external width. Controls were assessed at corresponding suprarenal abdominal aorta. ***$P < 0.001$, ****$P < 0.0001$, Welch ANOVA with Dunnett's T3 post hoc test, and mean ± SEM. (*B* and *C*) PDE1C$^{+/+}$ApoE$^{-/-}$ ($n = 6$) and PDE1C$^{-/-}$ApoE$^{-/-}$ ($n = 6$) with saline infusion. PDE1C$^{+/+}$ApoE$^{-/-}$ ($n = 21$) and PDE1C$^{-/-}$ApoE$^{-/-}$ ($n = 20$) with Ang II infusion. (*D*) Percentage survival curve. *$P < 0.05$, Mantel–Cox test, and PDE1C$^{+/+}$ApoE$^{-/-}$ ($n = 14$) and PDE1C$^{-/-}$ApoE$^{-/-}$ ($n = 13$) with Ang II infusion. (*E*) Representative VVG staining of cross-sections at AAA or at control suprarenal abdominal aorta. (*F*) Elastin degradation score. ***$P < 0.001$, Mann–Whitney *U* test between PDE1C$^{+/+}$ApoE$^{-/-}$ Ang II and PDE1C$^{-/-}$ApoE$^{-/-}$ Ang II, mean ± SEM, PDE1C$^{+/+}$ApoE$^{-/-}$ ($n = 6$) and PDE1C$^{-/-}$ApoE$^{-/-}$ ($n = 6$) with saline infusion, and PDE1C$^{+/+}$ApoE$^{-/-}$ ($n = 9$) and PDE1C$^{-/-}$ ApoE$^{-/-}$ ($n = 9$) with Ang II infusion.

(16). These results indicate that PDE1C deficiency reduces the susceptibility to develop AAA in vivo.

PDE1C Deficiency Attenuates AAA Development Induced by Periaortic Elastase Application. To further confirm the role of PDE1C in AAA development, we used a different mouse AAA model induced by periaortic elastase application combined with feeding 3-aminopropionitrile fumarate salt (BAPN) daily via drinking water (*SI Appendix*, Fig. S6) (17). Porcine pancreatic elastase breaks down aortic elastin. BAPN is an irreversible inhibitor of lysyl oxidase that is critical in maintaining homeostasis of elastic lamina. This model has been reported to resemble many features of human AAA, including the progressive expansion of infrarenal aorta, elastin fragmentation and degradation, loss of media SMC, and inflammation (17). PDE1C$^{+/+}$and PDE1C$^{-/-}$ male mice at the age of 9-wk-old under C57BL/6J background were used (*SI Appendix*, Fig. S7*A*). Twenty-eight days after surgery, PDE1C$^{-/-}$ mice with elastase displayed significant less dilation in abdominal aorta compared to PDE1C$^{+/+}$ mice (Fig. 3 *A* and *B*). *SI Appendix*, Fig. S7*B* includes images of all AAA samples shown in Fig. 3*B*. AAA of PDE1C$^{-/-}$ mice displayed less remarkable elastin damage compared to PDE1C$^{+/+}$ mice (Fig. 3 *C* and *D*). The arbitrary scale of elastin degradation semiquantitative analysis is shown in *SI Appendix*, Fig. S8. These data indicate that PDE1C deficiency plays a protective role in periaortic elastase-induced AAA and confirmed the causative role of PDE1C in AAA progression in vivo.

PDE1 Inhibitor Suppresses AAA Progression of Preestablished AAA. Next, we examined the pharmacological effect of a pan-PDE1 inhibitor IC86340 on the progression of preestablished moderate AAA using the periaortic elastase model. Based on the noninvasive color Doppler ultrasound analysis, AAA expansion in wild-type C57BL/6J mice was significantly developed by 7-d postsurgery (>50% normal abdominal aorta width) and further increased by 28 d compared to sham mice (*SI Appendix*, Fig. S6*A*). Thus, AAAs were first induced in C57BL/6J wild-type mice for 7 d. Mice were then randomly grouped and treated daily with IC86340 (6 mg/kg/d) or vehicle via intraperitoneal injection for 21 d (*SI Appendix*, Fig. S9*A*) (18). No difference in the gross morphology of sham aortas was observed between vehicle and IC86340 injection. IC86340 treatment limited AAA expansion effectively by 29% compared to vehicle (Fig. 3*E*). *SI Appendix*, Fig. S9*B* includes images of all AAA samples shown in Fig. 3*E*. VVG staining showed less elastin degradation in IC86340-treated AAA compared to vehicle group (Fig. 3*F* and *SI Appendix*, Fig. S10). These results suggest the therapeutic significance of PDE1 inhibition as a potential target in combating preestablished AAA.

PDE1C Promotes Mouse Aortic SMC Senescence. In our effort to culture mouse aortic SMCs from PDE1C$^{+/+}$ and PDE1C$^{-/-}$ mice, we found that PDE1C$^{-/-}$ SMCs could be maintained in culture for a significantly longer time than PDE1C$^{+/+}$ SMCs. A previous study reported increased PDE1C expression in cultured senescent human vascular SMCs (14). These clues suggest that PDE1C may regulate SMC senescence. Given the potential implications of cellular senescence in vascular aging and AAs (6, 7), we investigated the role of PDE1C in SMC senescence. SMC senescence was assessed by multiple senescent biomarkers, including senescence-associated β-galactosidase activity (SA–β-gal), p21 protein level, and γ-H2AX foci number (19). SA–β-gal activity is the mostly widely used senescent biomarker. It serves as a surrogate marker for the enhanced lysosomal content in senescent cells, which become detectable at a suboptimal pH of 6.0. p21 is a cyclin-dependent kinase inhibitor that is generally accumulated in senescent cells. DNA double strand breaks are

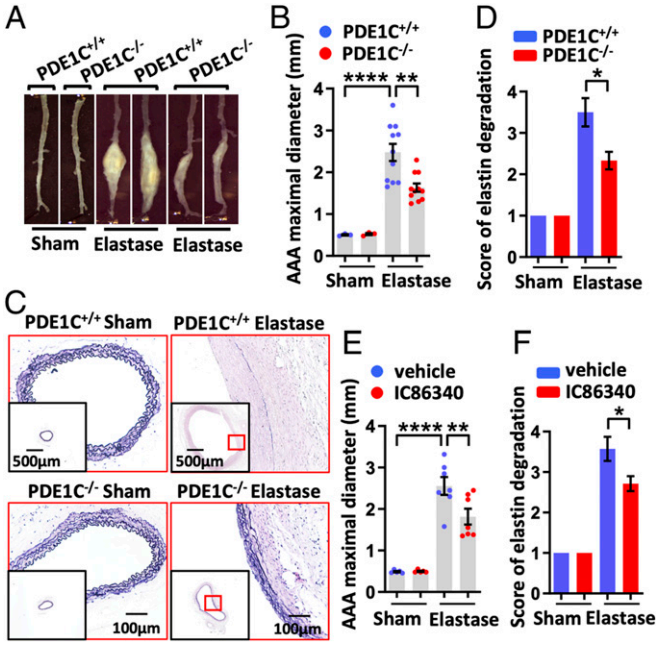

Fig. 3. PDE1C deficiency attenuates AAA development induced by periaortic elastase application, and PDE1 inhibition suppresses AAA progression of preestablished AAA. The 9-wk-old male PDE1C$^{+/+}$ and PDE1C$^{-/-}$ mice were applied with elastase (to induce AAA) or sham (as controls) at infrarenal abdominal aorta. (*A*) Representative images of infrarenal abdominal aorta at 4 wk postsurgery. (*B*) AAA maximal diameter of external width. Sham controls were assessed at corresponding infrarenal abdominal aorta. $^{**}P < 0.01$, $^{****}P < 0.0001$, Welch ANOVA with Dunnett's T3 post hoc test, mean ± SEM, PDE1C$^{+/+}$ ($n = 3$) and PDE1C$^{-/-}$ ($n = 3$) with sham, and PDE1C$^{+/+}$ ($n = 11$) and PDE1C$^{-/-}$ ($n = 11$) with elastase. (*C*) Representative VVG staining of cross-sections at AAA or at control infrarenal abdominal aorta. (*D*) Elastin degradation score. $^{*}P < 0.05$, Mann–Whitney *U* test between PDE1C$^{+/+}$ elastase and PDE1C$^{-/-}$ elastase, mean ± SEM, PDE1C$^{+/+}$ ($n = 3$) and PDE1C$^{-/-}$ ($n = 3$) with sham, and PDE1C$^{+/+}$ mice ($n = 6$) and PDE1C$^{-/-}$ mice ($n = 6$) with elastase. (*E* and *F*) Postintervention by PDE1 inhibition in periaortic elastase-induced AAA progression. (*E*) AAA maximal diameter of external width. $^{**}P < 0.01$, $^{****}P < 0.0001$, one-way ANOVA with Holm– Šídák's post hoc test, and mean ± SEM. Vehicle ($n = 5$) and IC86340 ($n = 5$) with sham, Vehicle ($n = 7$) and IC86340 ($n = 7$) with elastase. (*F*) Elastin degradation score. $^{*}P < 0.05$, Mann–Whitney *U* test between elastase vehicle and elastase IC86340, and mean ± SEM. Vehicle ($n = 3$) and IC86340 ($n = 3$) with sham, Vehicle ($n = 27$) and IC86340 ($n = 7$) with elastase.

often reported as a commonly underlying cause of senescence and lead to phosphorylation of histone H2A.X^{Ser139}, known as γ-H2AX. We found that primary cultured mouse aortic SMCs isolated from PDE1C$^{+/+}$ mice revealed an intrinsically higher level of senescence compared to PDE1C$^{-/-}$ SMCs, as quantified by SA–β-gal–positive cell numbers over total cell numbers (Fig. 4 *A* and *B*). Overexpressing PDE1C1, a variant expressing in SMCs (12), in PDE1C$^{-/-}$ SMCs promoted senescence via adenovirus (Fig. 4*C*). Double staining of p21 and SA–β-gal activity were further performed in PDE1C$^{+/+}$ and PDE1C$^{-/-}$ SMCs (Fig. 4*D*), and PDE1C$^{-/-}$ SMCs displayed less double-positive cells (Fig. 4*E*). The staining specificity was supported by negative control of p21 immunostaining (*SI Appendix*, Fig. S11*A*) and the neglectable autofluorescence of SA–β-gal staining alone (*SI Appendix*, Fig. S11*B*). Western blot (WB) further confirmed a lower level of p21 protein expression in PDE1C$^{-/-}$ compared to PDE1C$^{+/+}$ SMCs (Fig. 4*F*). Additionally, γ-H2AX immunostaining (Fig. 4*G* and *SI Appendix*, Fig. S12) revealed less γ-H2AX foci number in PDE1C$^{-/-}$ SMC nucleus (Fig. 4*H*), indicating less DNA damage. Together, these results support a critical role of PDE1C in SMC senescence in vitro.

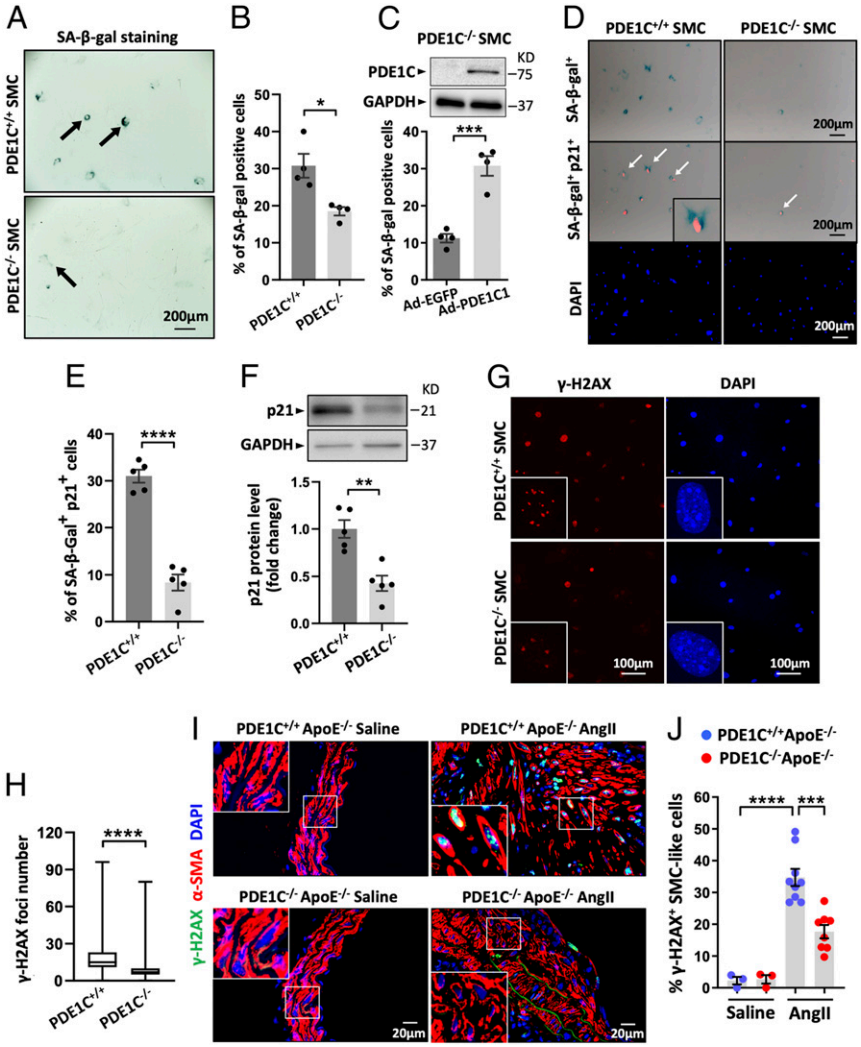

Fig. 4. PDE1C promotes mouse aortic SMC senescence. (*A–H*) Aortic SMCs isolated from 10-wk-old PDE1C$^{+/+}$ or PDE1C$^{-/-}$ mice via enzymatic digestion. (*A* and *B*) Representative images of SA–β-gal activity staining and the percentage of positively stained cells (blue) over total cell number. *$P < 0.05$, unpaired Student's *t* test, mean ± SEM, and $n = 4$ separate experiments. (*C*) PDE1C$^{-/-}$ SMCs were transduced with Ad-mPDE1C1-Flag (Ad-PDE1C1) to reconstitute PDE1C or transduced with Ad-EGFP as control. (*Upper*) PDE1C protein levels by WB. (*Lower*) Percentage of SA–β-gal–positive cells. ***$P < 0.001$, unpaired Student's *t* test, mean ± SEM, and $n = 4$ separate experiments. (*D* and *E*) Representative images of SA–β-gal (blue) and p21 (red) double staining and the percentage of double-positive cells over total cell number. Nuclei were stained with DAPI. ****$P < 0.0001$, unpaired Student's *t* test, mean ± SEM, and $n = 5$ separate experiments. (*F*) p21 protein levels by WB. **$P < 0.01$, unpaired Student's *t* test, mean ± SEM, and $n = 5$ separate experiments. (*G* and *H*) Representative images of γ-H2AX (red) immunostaining and DAPI (nuclei) and the γ-H2AX foci number in each cell. ****$P < 0.0001$, Mann–Whitney *U* test, median with interquartile range, and a total of 280 to 350 cells were included from four separate experiments. (*I* and *J*) Representative images of γ-H2AX and α-SMA immunostaining in cross-sections of AAA induced by Ang II or control abdominal aortas and the percentage of double positively stained cell number over total SMC-like cell (α-SMA$^+$) number. Each dot represents an individual mouse. ***$P < 0.001$, ****$P < 0.0001$, one-way ANOVA with Holm–Šídák's post hoc test, and mean ± SEM. PDE1C$^{+/+}$ApoE$^{-/-}$ ($n = 3$) and PDE1C$^{-/-}$ApoE$^{-/-}$ ($n = 3$) with saline, PDE1C$^{+/+}$ApoE$^{-/-}$ ($n = 9$) and PDE1C$^{-/-}$ ApoE$^{-/-}$ ($n = 8$) with Ang II.

We next performed double immunostaining of γ-H2AX and α-SMA in cross-sections of suprarenal abdominal aorta from PDE1C$^{+/+}$ApoE$^{-/-}$ and PDE1C$^{-/-}$ApoE$^{-/-}$ mice infused with saline (control) or Ang II (AAA). Compared to control aortas, AAA tissues from PDE1C$^{+/+}$ApoE$^{-/-}$ mice showed dramatic numbers of colocalization of γ-H2AX with α-SMA (Fig. 4*I*), indicating SMC-like cells in AAA displayed more senescence. The increased γ-H2AX signal in AAA of PDE1C$^{+/+}$ApoE$^{-/-}$ mice was largely alleviated in AAA of PDE1C$^{-/-}$ApoE$^{-/-}$ mice (Fig. 4 *I* and *J* and *SI Appendix*, Figs. S13 and S14), suggesting that PDE1C deficiency reduced SMC senescence in AAA.

PDE1C Regulates Human Aortic SMC Senescence. We also determined the role of PDE1C in human aortic SMC senescence. Primary human SMCs isolated from normal human aorta or human AAA were cultured. Compared to normal SMCs, AAA SMCs exhibited higher levels of PDE1C mRNA (Fig. 5*A*) and protein (Fig. 5*B*). This was associated with higher SA–β-gal activity staining (Fig. 5 *C* and *D*), indicating a more senescent phenotype of human AAA SMCs.

Ang II (as aging stimulator) or H_2O_2 (as oxidative stress inducer) are often used as in vitro cell model to induce senescence (20, 21). In normal human aortic SMCs, Ang II treatment upregulated PDE1C mRNA and protein levels time-dependently (Fig. 5 *E* and *F*) and dose-dependently (*SI Appendix*, Fig. S15*A*). Knockdown (KD) of PDE1C expression (~80%) by small interfering RNA (siRNA) (siPDE1C) (*SI Appendix*, Fig. S15*B*) significantly reduced Ang II–induced SMC senescence, as indicated by lower SA–β-gal activity staining (Fig. 5*G* and *SI Appendix*,

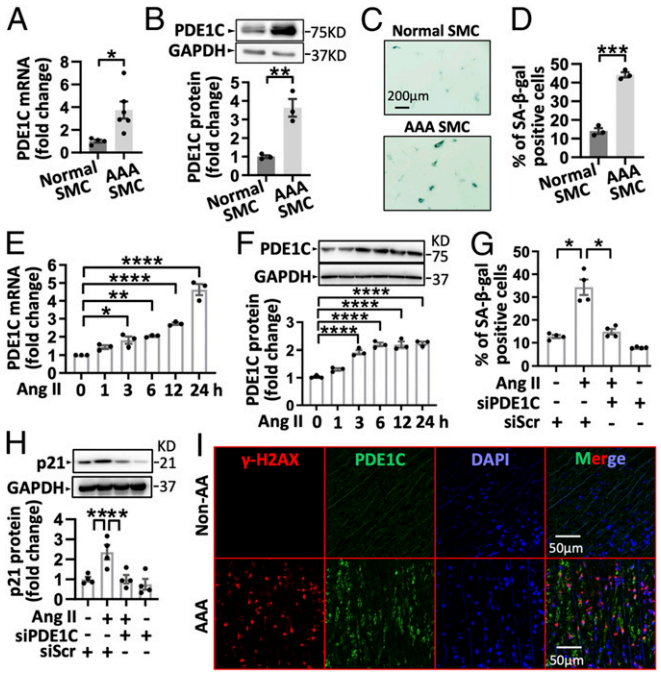

Fig. 5. PDE1C regulates human SMC senescence. (*A–D*) Aortic SMCs were isolated and cultured from human normal aortas or human AAA. (*A*) PDE1C mRNA levels by qPCR, normalized to GAPDH. $*P < 0.05$, Welch's *t* test, mean ± SEM, and four to six culture replicates were included in two separate qPCR experiments. (*B*) PDE1C protein levels by WB. $**P < 0.01$, unpaired Student's *t* test, mean ± SEM, and $n = 3$ separate experiments. (*C* and *D*) Percentage of SA–β-gal–positive cells. $***P < 0.001$, unpaired Student's *t* test, mean ± SEM, and $n = 3$ separate experiments. (*E–H*) Human normal aortic SMCs were cultured and stimulated with Ang II to induce senescence. (*E*) PDE1C mRNA levels by qPCR, normalized to GAPDH. $*P < 0.05$, $**P < 0.01$, $****P < 0.0001$, one-way ANOVA with Holm–Šídák's post hoc test, mean ± SEM, and $n = 3$ separate experiments. (*F*) PDE1C protein levels by WB. $****P < 0.0001$, one-way ANOVA with Holm–Šídák's post hoc test, mean ± SEM, and $n = 3$ separate experiments. (*G*) Percentage of SA–β-gal–positive cells in human SMCs with PDE1C siRNA (siPDE1C) or scramble siRNA (siScr) treatment. $*P < 0.05$, Welch ANOVA with Dunnett's T3 post hoc test, mean ± SEM, and $n = 4$ separate experiments. (*H*) p21 protein expression by WB with siPDE1C treatment. $**P < 0.01$, one-way ANOVA with Holm–Šídák's post hoc test, mean ± SEM, and $n = 4$ separate experiments. (*I*) Representative immunostaining of γ-H2AX and PDE1C in cross-sections of human nonaneurysmal abdominal aorta or human AAA. At least three different sets of human samples were performed at separate experiments with similar observations.

Fig. S15*C*) and decreased p21 protein level (Fig. 5*H*). Similarly, H_2O_2 stimulation elevated PDE1C protein expression in normal human aortic SMC dose-dependently (*SI Appendix*, Fig. S16*A*). H_2O_2 also stimulated human SMC senescence, which was diminished by siPDE1C treatment (*SI Appendix*, Fig. S16 *B–D*).

Double immunostaining of γ-H2AX and PDE1C was performed in human AAA and non-AAA tissues. In the medial areas, there were abundant cells positive of γ-H2AX and PDE1C staining in AAA compared to non-AAA (Fig. 5*I* and *SI Appendix*, Fig. S17). This suggests that PDE1C induction in human AAA was associated with SMC senescence.

SIRT1 Is a Critical Mediator for PDE1C-Mediated Regulation of SMC Senescence In Vitro. SIRT1 is a longevity gene that encodes a NAD^+-dependent protein deacetylase. SIRT1 plays important roles in many cellular functions, including cell senescence (22). SIRT1 is highly expressed in vasculature and has been suggested to suppress SMC senescence and AAA (7). Also, cAMP can directly or indirectly regulate SIRT1 expression and/or activation (23, 24). Given these clues, we examined the role of SIRT1 in the PDE1C-mediated regulation of SMC senescence. Cell senescence was significantly reduced in $PDE1C^{-/-}$ SMCs compared to $PDE1C^{+/+}$ cells, which was reversed by two different SIRT1 selective inhibitors, EX-527 (Fig. 6*A*) or (S)-35 (Fig. 6*B*). The SIRT1 protein level was higher in $PDE1C^{-/-}$ SMCs compared to $PDE1C^{+/+}$ SMCs (Fig. 6*C*). Overexpressing PDE1C1 via adenovirus in $PDE1C^{-/-}$ SMCs reduced SIRT1 protein levels compared to the GFP control (Fig. 6*D*).

In normal human aortic SMCs, KD of PDE1C with siPDE1C also increased SIRT1 protein levels at basal (Fig. 6*E*) and Ang II–stimulated states (Fig. 6*F*). siPDE1C significantly antagonized Ang II–induced SMC senescence, which was partially blocked by KD of SIRT1 with SIRT1 selective siRNA (siSIRT1) (Fig. 6*G* and *SI Appendix*, Fig. S18*A*). The siSIRT1 blocked SIRT1 upregulation by siPDE1C, which confirmed the KD efficiency of siSIRT1 (*SI Appendix*, Fig. S18*B*). Consistently, siSIRT1 also blocked the effect of siPDE1C on H_2O_2-induced SMC senescence (*SI Appendix*, Fig. S18 *C* and *D*).

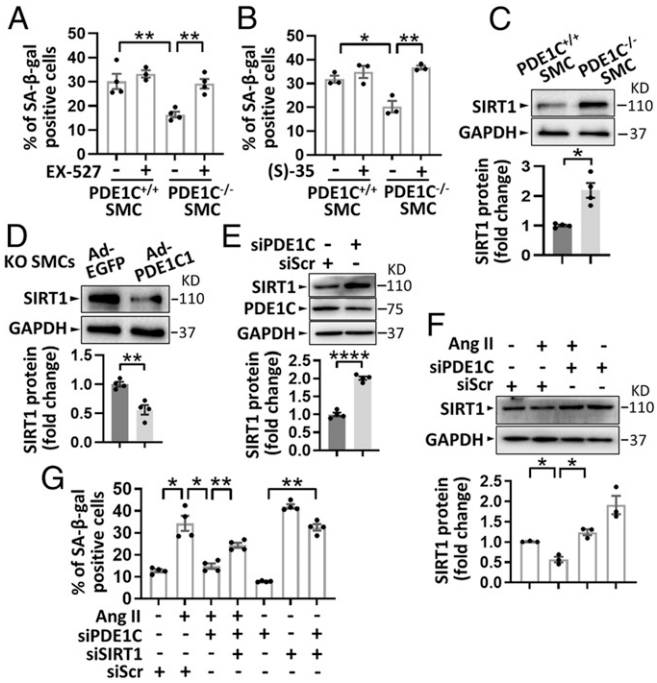

Fig. 6. SIRT1 is a critical mediator for PDE1C-mediated regulation of SMC senescence in vitro. (*A–D*) Mouse aortic SMCs isolated from $PDE1C^{+/+}$ or $PDE1C^{-/-}$ mice were used. (*A*) Percentage of SA–β-gal–positive cells in SMCs treated with SIRT1 inhibitor EX-527 (30 μM) for 7 d. $**P < 0.01$ and one-way ANOVA with Holm–Šídák's post hoc test. $n = 4$ separate experiments. (*B*) Percentage of SA–β-gal–positive cells in SMCs treated with SIRT1 inhibitor (S)-35 (20 μM) for 7 d. $*P < 0.05$, $**P < 0.01$, and one-way ANOVA with Holm–Šídák's post hoc test. $n = 3$ separate experiments. (*C*) SIRT1 protein expression by WB. $*P < 0.05$ and Welch's *t* test. $n = 4$ separate experiments. (*D*) SIRT1 protein expression in $PDE1C^{-/-}$ SMCs transfected with adenovirus Ad-EGFP (control) or Ad-mPDE1C1-flag (Ad-PDE1C1) (PDE1C overexpression). $**P < 0.01$ and unpaired Student's *t* test. $n = 4$ separate experiments. (*E*) SIRT1 protein expression by WB in human aortic SMC treated with siPDE1C. $****P < 0.0001$ and Welch's *t* test. $n = 4$ separate experiments. (*F*) SIRT1 protein expression by WB in human aortic SMC treated with Ang II and siPDE1C. $*P < 0.05$ and one-way ANOVA with Holm–Šídák's post hoc test. $n = 3$ separate experiments. (*G*) Percentage of SA–β-gal–positive human aortic SMC treated with Ang II and siPDE1C and/or SIRT1 siRNA (siSIRT1). $*P < 0.05$, $**P < 0.01$, and Welch ANOVA with Dunnett's T3 post hoc test. $n = 4$ separate experiments. All data in this figure are represented mean ± SEM.

SIRT1 Is Critical in PDE1C Regulation of AAA In Vivo. To establish the relationship of PDE1C and SIRT1 in vivo, we compared SIRT1 level in control and AAA tissues. We found that mouse AAA induced by Ang II infusion displayed less SIRT1 immunostaining intensity in the medial area compared to abdominal aorta of saline-infused mice, while this was reversed in PDE1C$^{-/-}$ mice (Fig. 7 *A* and *B* and *SI Appendix*, Fig. S19*A*). A similar result was obtained in mouse AAAs induced by periaortic elastase (*SI Appendix*, Fig. S19 *B* and *C*). Consistently, human AAA also exhibited less SIRT1 protein compared to control aortas, as assessed by WB (Fig. 7*C*) and immunostaining at medial areas (Fig. 7 *D* and *E* and *SI Appendix*, Fig. S20 show more examples). Together, these results indicate a connection of PDE1C and SIRT1 in AAA.

Having found the role of SIRT1 in PDE1C-regulated SMC senescence in vitro and the relationship between PDE1C and SIRT1 in AAA tissues, we examined the effect of SIRT1 inhibition on the PDE1C-mediated regulation of AAA in vivo using the periaortic elastase model. PDE1C$^{+/+}$ or PDE1C$^{-/-}$ mice were provided with BAPN and periaortic elastase surgery to induce AAA. Pluronic gel containing either SIRT1 inhibitor EX527 or vehicle was applied perivascularly on abdominal aorta after elastase treatment. AAA dilation was examined 4-wk postsurgery (*SI Appendix*, Fig. S21*A*). We found that the local SIRT1 inhibitor application partially reversed the protective effect of PDE1C deficiency against AAA dilation (Fig. 7 *F* and *G*), suggesting a functional role of SIRT1 in PDE1C-regulated AAA development. *SI Appendix*, Fig. S21*B* includes images of all AAA samples shown in Fig. 7*G*. It is worth mentioning that the effect of EX527 may be lessened because of the limitation of the EX527 application method.

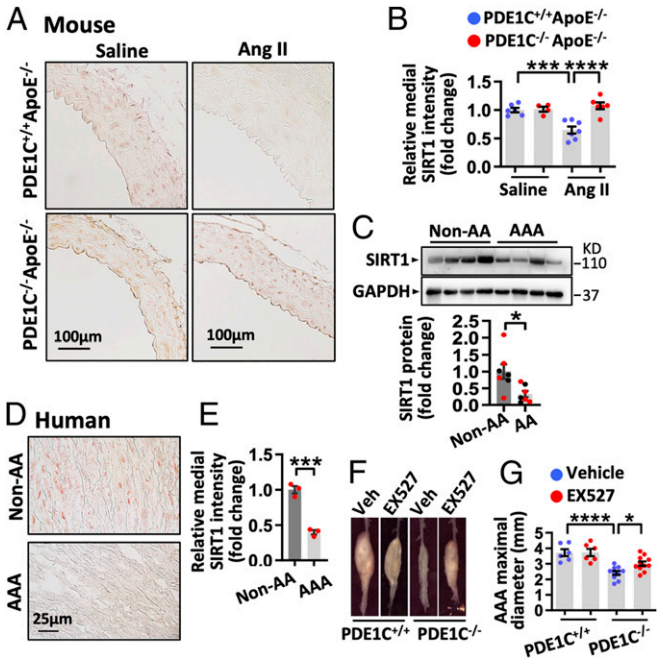

Fig. 7. SIRT1 is critical in PDE1C regulation of AAA in vivo. (*A*) Representative images of SIRT1 immunostaining in cross-sections of abdominal aorta from saline or Ang II infusion mice. (*B*) Quantification of SIRT1 staining intensity at media. Each dot represents an individual mouse. ***$P < 0.001$, ****$P < 0.0001$, and one-way ANOVA with Holm–Šídák's post hoc test. (*C–E*) Human AAA (red dots) and aneurysm at other aortic locations (black dots) were used as AA samples. Human nonaneurysmal aorta at abdominal (red dots) and at other aortic locations (black dots) were used as controls. (*C*) SIRT1 protein levels by WB. *Upper* is the representative WB image, and *Bottom* is the quantified results. $P = 0.125$ abdominal controls versus AAA, unpaired Student's *t* test, abdominal controls ($n = 4$), and AAA ($n = 4$). *$P < 0.05$ controls versus AA, unpaired Student's *t* test, controls ($n = 7$), and AA ($n = 7$). (*D*) Representative images showing immunostaining of SIRT1 in cross-sections of human nonaneurysmal abdominal aorta and human AAA. (*E*) Quantification of SIRT1 staining intensity at media. Each dot represents an individual person. ***$P < 0.001$, unpaired Student's *t* test, abdominal controls ($n = 3$), and AAA ($n = 3$). (*F* and *G*) PDE1C$^{+/+}$ or PDE1C$^{-/-}$ mice were subjected to elastase/BAPN treatment to induce AAA and perivascularly applied with Pluronic gel containing DMSO (control) or EX527 (SIRT1 inhibitor, 50 μM). (*F*) Representative images of infrarenal abdominal aorta at 4 wk postsurgery. (*G*) AAA maximal diameter of external width. *$P < 0.05$, ****$P < 0.0001$, one-way ANOVA with Holm–Šídák's post hoc test, control ($n = 6$) and EX527 ($n = 6$) for PDE1C$^{+/+}$, and control ($n = 10$) and EX527 ($n = 11$) for PDE1C$^{-/-}$. All data in this figure are represented mean ± SEM.

PDE1C-Regulated cAMP Directly Binds and Activates SIRT1. PDE1C can hydrolyze both cAMP and cGMP with high affinity in cell-free system (8). Inside of cells, PDE1C regulation of cAMP, cGMP, or both is dependent on its association with cAMP or/and cGMP signaling complex. The canonical cAMP and cGMP effectors include protein kinase A (PKA), exchange protein activated by cAMP (Epac), and PKG. We first determined whether any of these is involved in PDE1C-mediated regulation of SMC senescence. We found that PKA inhibitor PKI, Epac inhibitor ESI-09, or PKG inhibitor DT2 did not significantly change the effects of PDE1C deficiency on SMC senescence (*SI Appendix*, Fig. S22 *A–C*), suggesting that PDE1C-regulated SMC senescence might be mediated through a noncanonical cyclic nucleotide signaling.

The findings from the previous study have suggested that cAMP exerts an anti-aging effect and may directly bind and activate SIRT1 (23). To determine whether cAMP is critical for PDE1C-regulated SMC senescence, we first blocked cAMP production with different pan-inhibitors of membrane adenylyl cyclase (mAC), SQ22536 and NKY80. We found that the inhibitory effect of PDE1C deficiency on SMC senescence was reversed by either NKY80 (Fig. 8*A*) or SQ22536 (Fig. 8*B*), suggesting that cAMP derived from mAC is important in the PDE1C-mediated regulation of SMC senescence. We next determined whether PDE1C regulates SIRT1 activity. We overexpressed SIRT1 in wild-type SMCs via adenovirus and acutely treated SMCs with PDE1 inhibitor IC86340 for 30 min. We found that IC86340 treatment increased cellular SIRT1 activity, indicating that a rapid response of PDE1 inhibition promotes SIRT1 activation (Fig. 8*C*).

To examine whether PDE1C-regulated cAMP directly interacts with SIRT1, we first performed double immunostaining for cAMP and SIRT1 in wild-type mouse SMCs treated with IC86340 for 30 min. Confocal microscopy showed that PDE1 inhibition increased cAMP staining and the colocalization of cAMP and SIRT1, but did not change the SIRT1 staining (Fig. 8 *D* and *E* and *SI Appendix*, Fig. S22*D*). To further confirm the direct physical interaction between cAMP and SIRT1, we used proximity ligation assays (PLAs) that involve the use of two specific primary antibodies, respectively, against cAMP and SIRT1, and the pair of secondary antibodies bears complementary oligonucleotides, which will be annealed into a circular double stranded DNA molecule upon close proximity. After amplification, the signal from each pair of PLA probes is detected with a fluorescent dye-labeled probe and visualized as an individual red fluorescent dot under microscope (*SI Appendix*, Fig. S23*A*). We observed more PLA signals per cell in SMCs treated with IC86340, indicating more cAMP–SIRT1 interaction (Fig. 8 *F* and *G* and *SI Appendix*, Fig. S23*B*). In vivo, mouse AAA induced by Ang II showed remarkably less PLA signal in the medial area compared to saline-infused controls, whereas the PLA signal was partially preserved in AAA of PDE1C$^{-/-}$ mice (Fig. 8 *H* and *I* and *SI Appendix*, Fig. S23*C*). These results indicate that PDE1C-regulated cAMP directly interacts with SIRT1 in SMCs.

Next, we sought to understand how PDE1C regulates SIRT1 expression through directly acting on SIRT1 activity. Several previous studies have suggested that SIRT1 activation can drive SIRT1 expression (25, 26). We found that inhibition of SIRT1

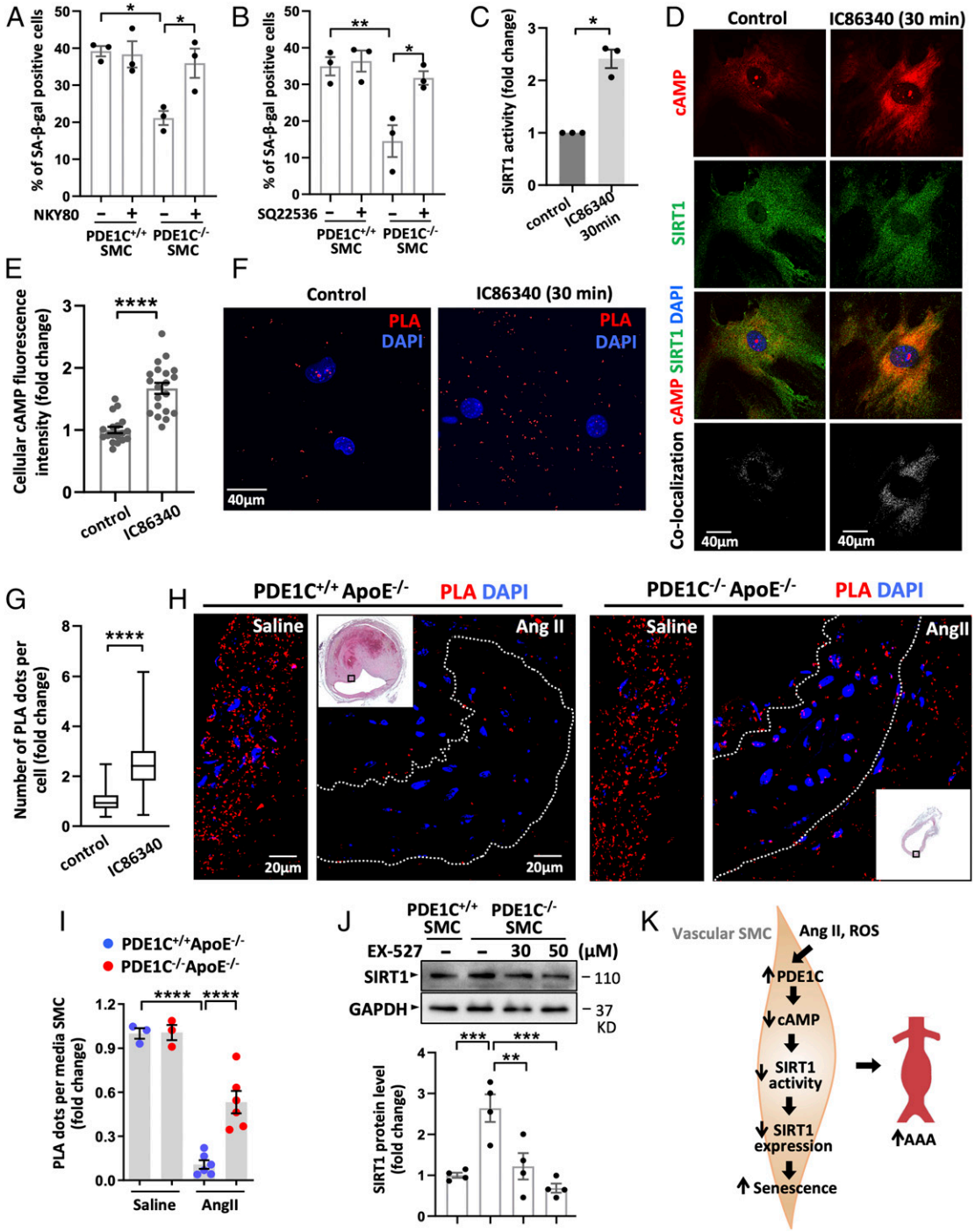

Fig. 8. PDE1C-regulated cAMP directly binds and activates SIRT1. (*A* and *B*) Percentage of SA–β-gal–positive mouse PDE1C$^{+/+}$ or PDE1C$^{-/-}$ SMCs treated with mAC inhibitor NKY80 (20 μM) or SQ22536 (80 μM), as indicated, for 7 d. *$P < 0.05$, **$P < 0.01$, one-way ANOVA with Holm–Šídák's post hoc test, mean ± SEM, and $n = 3$ separate experiments. (*C–G*) Wild-type mouse aortic SMC were treated with DMSO (control) or PDE1 inhibitor IC86340 (15 uM) for 30 min. (*C*) SIRT1 activity. SIRT1 was overexpressed in rat SMCs via adenovirus, and cellular SIRT1 activity was assayed. *$P < 0.05$, Welch's t test, mean ± SEM, and $n = 3$ separate experiments. (*D*) Representative images of coimmunostaining of cAMP and SIRT1. Colocalization analysis revealed a colocalized signal in white. (*E*) Quantification of cAMP fluorescence intensity shown in *D*. Each dot represents the intensity in one cell. ****$P < 0.0001$, Welch's t test, and mean ± SEM. (*F*) Representative images showing PLA signals of cAMP and SIRT1. (*G*) Quantification of PLA dots per cell. ****$P < 0.0001$, Mann–Whitney U test, median with interquartile range, and ∼150 cells were counted from three separate experiments. (*H*) Representative PLA signals of cAMP and SIRT1 in cross-sections of control abdominal aorta or AAA in PDE1C$^{+/+}$ApoE$^{-/-}$ and PDE1C$^{-/-}$ApoE$^{-/-}$ mice infused with saline or Ang II. The area surrounded by the white dotted lines indicates the media layer. Insets are hematoxylin and eosin (H&E) staining of the adjacent section. The boxed area in H&E shows the magnified area by PLA. (*I*) Quantification result showing PLA dots per medial cell. Each dot in the bar graph represents an individual mouse. ****$P < 0.0001$, one-way ANOVA with Holm–Šídák's post hoc test, and mean ± SEM. (*J*) SIRT1 protein level by WB in PDE1C$^{+/+}$ or PDE1C$^{-/-}$ SMCs treated with EX527. **$P < 0.01$, ***$P < 0.001$, one-way ANOVA with Holm–Šídák's post hoc test, mean ± SEM, and $n = 4$ separate experiments. (*K*) Proposed model: PDE1C antagonizes cAMP-mediated activation of SIRT1 and subsequently promotes SMC senescence and AAA development.

activity by EX-527 diminished SIRT1 expression in SMCs (Fig. 8*J*). This suggests that there is perhaps a positive feedback loop in SMCs that drive SIRT1 expression via its own activity.

Discussion

The major goal of this study is to explore the regulation, function, and underlying mechanism of PDE1C isozyme in AAA development by focusing on SMC senescence. Using genetic and pharmacological approaches, we have demonstrated that PDE1C induction plays a causative role in AAA development, at least partially through antagonizing the cAMP-mediated activation of SIRT1 and subsequently promoting SMC senescence (Fig. 8*K*). We also showed that the pan-PDE1 inhibitor IC86340 significantly attenuated AAA progression of preexisting moderate AAA in mice (Fig. 3 *E* and *F*). IC86340 inhibits all three PDE1 isozymes. Among them, PDE1A and PDE1C, but not PDE1B, are expressed in human and rodent contractile and/or synthetic SMCs (12, 27). Different from PDE1C, PDE1A is found in both contractile and synthetic SMCs (27). However, the role of SMC PDE1A in AAA remains unknown. Besides SMCs, macrophages are also important for the AAA development. It has been reported that PDE1B represents the major PDE1 activity in macrophages (28), and PDE1C is not detected in mouse peritoneal macrophages (11). Therefore, the contributions of PDE1A and/or PDE1B could not be completely excluded from the effect of IC86340 on AAA. Currently, another pan-PDE1 inhibitor ITI-214 has been under development for treating schizophrenia as well as under clinical trial phase 2 for heart failure (ClinicalTrials.gov Identifier: NCT03387215), suggesting the potential safety of using PDE1 inhibitors as therapeutic agents. Taken together, our study demonstrates a role of PDE1C in AAA development and a mechanistic action of PDE1C in regulating SIRT1 activity and cell senescence. Our findings may facilitate the development of PDE1 inhibitors as therapeutic agents for treating aneurysm, as well as provide insight into the potential vascular side effects when using PDE1 inhibitors in treating other diseases.

The studies of cAMP signaling in aneurysm are still scattered and inadequate. A previous study reported that SMC-specific KO of cAMP-generating G protein ($G_{s\alpha}$) exaggerated AAA in mice (9). However, the role of G protein–coupled receptors (GPCRs) that activates $G_{s\alpha}$ in SMCs and AAA remains poorly understood. Cilostazol has been shown to suppress AAA in rat and mouse (29). In addition to being a PDE3 inhibitor that increases cAMP level, cilostazol also inhibits adenosine uptake and increases interstitial and circulatory adenosine (30). It is believed that the augmentation of adenosine function by cilostazol minimizes its cardiac effect resulted from inhibiting PDE3 during the clinical treatment for intermittent claudication (30). Future studies are required to clarify the mechanistic actions of cilostazol on AAA: cAMP or adenosine. Herein, we showed that PDE1C inactivation, likely by potentiating a unique cAMP signaling, inhibits AAA (Fig. 8). Thus, these findings together suggest that some of cAMP signaling may be protective against AAA. In vascular SMCs, there are a number of different $G_{s\alpha}$-coupled GPCRs and cAMP-hydrolyzing PDEs, which may lead to stimulating multiple spatially discrete and functionally distinct cAMP signaling in SMCs. It remains unclear whether distinct cAMP signaling function differentially in AAA, which warrant to be explored in the future with specific GPCR agonist/antagonist, PDE isozyme-specific activator/inhibitor, and/or gene-specific transgenic/KO mice.

It has long been believed that myofibroblast-like, α-SMA–positive cells in vascular lesions are derived from the phenotypic modulation of contractile, medial SMCs. However, evidence also supports the transdifferentiation to myofibroblasts from adventitial fibroblasts (31), progenitor cells (32), or ECs (33). Regardless of origins, synthetic, SMC-like cells are evidently proliferatory, migratory, secretory, inflammatory, and apoptotic, playing key roles in various types of pathological vascular remodeling, such as in neointimal (11), atherogenic (12), and aneurysmal tissues (2). In addition to SMCs, PDE1C in other nonvascular tissues may also indirectly affect AAA development, which is the limitation of our current study with a global PDE1C KO mice. Nevertheless, the findings of our current study using global PDE1C KO mice, as well as the systemic application of the PDE1 inhibitor, provide insight into the potential of targeting PDE1C in antagonizing AAA development, which has significant pharmacological significance.

We have previously shown that PDE1C is important for SMC proliferation, migration, and neointimal hyperplasia, in part through negatively modulating PDGFR-β protein endocytosis/degradation and thus promoting PDGFR-β signaling (11). This function of PDE1C is mediated by mAC/cAMP and PKA-dependent phosphorylation of low-density lipoprotein receptor–related protein-1 (11). We have also found that PDE1C regulates lysosome-mediated collagen I protein degradation through a soluble adenylyl cyclase/cAMP/PKA signaling (34). In the current study, we discovered that PDE1C regulates SIRT1 activation and SMC senescence via a cAMP-dependent, while PKA-independent, mechanism by which cAMP directly binds with SIRT1 and promotes SIRT1 activity. These results together suggest that PDE1C can regulate multiple functions of synthetic SMCs via distinct mechanisms. cAMP that binds to and activates SIRT1 has been investigated in a previous study with multiple biochemical approaches (23). For example, it has been shown that 1) cAMP increases SIRT1 activity in a cell-free system; 2) surface plasmon resonance detected direct binding between immobilized SIRT1 on a sensor chip with cAMP (KD = 1.05 μM); and 3) auto-dock analysis shows that cAMP occupies half of the NAD^+-binding pocket on SIRT1, and the catalytic site is available for the reaction between SIRT1 and NAD^+, which results in a higher rate of NAD^+ hydrolysis and improved reaction efficiency between NAD^+ and SIRT1. In our current study, we provided direct biological evidence to further support the interaction of cAMP and SIRT1 inside of SMCs upon cAMP elevation by inhibiting PDE1C. Recently, increasing evidence has indicated cAMP binding to proteins that do not have conventional, cyclic nucleotide-binding site(s). For example, dopamine receptor–derived cAMP binds to NLRP3 (NOD-, LRR-, and pyrin domain–containing protein 3), which destabilizes the NLRP3 protein and thus inhibits inflammasome activation (35).

In the current study, we induced AAA using two different models, including chronic Ang II infusion in $ApoE^{-/-}$ mice and perivascular elastase application combined with BAPN. These two models show multiple differences in anatomic positions, histological features, and pathological mechanisms (17). For example, Ang II infusion in $ApoE^{-/-}$ mice develops the suprarenal aorta AAA accompanied by atherosclerosis (15). Chronic inflammation appears to be a dominant mechanism in the Ang II infusion model. The destruction of elastic layers is usually a result of inflammation and reactive oxygen species in the middle phase (15). Perivascular elastase model induces infrarenal AAA (17). It involves an initial acute inflammation mainly in the adventitia and acute breakdown of elastic fibers due to elastase treatment (17). Despite the differences, the two models share some common AAA features, such as persistent aneurysm growth, leukocyte infiltration, ECM degradation, and medial layer degeneration (15, 17). To date, none of the rodent AAA models are identical to human AAAs, and different models resemble unique human features. Therefore, it is more appropriate using different animal models to strengthen findings. In addition to human AAAs, PDE1C up-regulation also occurs in AA at other parts of aortas (Fig. 1 *C* and *D*), suggesting that PDE1C may also contribute to other AAs. Thus, it will be of great interest to test PDE1C deficiency or inhibition in other AA models in the future.

Materials and Methods

A complete description of the methods is provided in *SI Appendix*, Materials and Methods.

Human Aorta Samples. AA tissue specimens were obtained from patients undergoing elective surgical repair of AAA (abdominal) or AA at other locations (nonabdominal). Age-matched nonaneurysmal aortic tissues were obtained from patients (aortic punch samples) undergoing coronary bypass surgery, kidney artery bypass surgery, or obtained from organ donors. The patient samples are deidentified and their characteristics are shown in *SI Appendix*, Table S1 and detailed in *SI Appendix, Materials and Methods*. The collection of human tissues and their use for research was approved by the ethical committee of Beijing AnZhen Hospital in China.

Animal Experiments. Mouse experiments followed protocols approved by University of Rochester Committee on Animal Resources. Double-KO (PDE1C$^{-/-}$ApoE$^{-/-}$) mice were derived from cross-breeding of global PDE1C$^{-/-}$ mice (11) with ApoE$^{-/-}$ mice. To induce AAAs, we performed two mouse models of Ang II–induced and periaortic elastase (17)–induced AAA. Details of animal experiments are described in *SI Appendix, Materials and Methods*.

Blood Pressure Measurement and Ultrasound Imaging. Systolic arterial blood pressure was monitored by using a noninvasive tail cuff plethysmography method. Diastole internal diameter in mouse was detected by a Vevo 2100 ultrasound imaging platform (FUJIFILM VisualSonics).

Aortic SMC Culture. Mouse aortic SMCs were isolated from 10-wk-old PDE1C$^{+/+}$ or PDE1C$^{-/-}$ mice via enzymatic digestion using elastase and type II collagenase, and cells were used from passages 6 to 10 for experiments. Primary aortic SMCs isolated from human AAA specimens or normal human aorta samples were subcultured and used from passages 5 to 7. Human normal aortic SMCs purchased (ScienCell Research Laboratories) were used for experiments between passage 2 and 5.

Histology, Immunostaining, and PLA. Paraffin aorta cross-sections were stained for VVG staining or immunofluorescence of PDE1C, α-SMA, γ-H2AX, or SIRT1. SMCs culture were stained for immunofluorescence of γ-H2AX, cAMP, or SIRT1 or stained for SA–β-gal activity alone or in combination of p21 immunostaining. PLA was performed in aorta cross-section or cultured SMCs to detect cAMP and SIRT1 interactions in situ based on the manufacturer's protocol.

SIRT1 Deacetylase Activity Assay. Rat aortic SMCs were transduced with adenovirus to express exogenous SIRT1 and treated with 15 μM IC86340 for 30 min. Cellular SIRT1 activity was detected using a SIRT1 activity assay kit according to manufacturer's instructions.

Statistical Analysis. Assumptions of normality and equal variance were tested using R. Shapiro–Wilk test was used to test for normal distribution. Brown–Forsythe test was used to test for equality of variances. All tests were two sided, with a significance level for two-sided tests set at 5%. Statistical analyses were conducted using GraphPad Prism 8. Detailed statistical methods are listed in *SI Appendix*, Table S2.

Data Availability. All study data are included in the article and/or *SI Appendix*.

ACKNOWLEDGMENTS. This work was financially supported by NIH Grants HL134910 and HL154318 (to C.Y.), American Heart Association fellowship 20PRE35210148 (to C.Z.), the National Key Research and Development Program of China Grants 2019YFA0801700 and 2019YFA0801800 (To J.W.), and the Chinese Academy Sciences Innovation Fund for Medical Sciences (Grant 2016-12M-1-006 to J.W).

1. N. Sakalihasan *et al*., Abdominal aortic aneurysms. *Nat. Rev. Dis. Primers* **4**, 34 (2018).
2. J. A. Curci, Digging in the "soil" of the aorta to understand the growth of abdominal aortic aneurysms. *Vascular* **17** (suppl. 1), S21–S29 (2009).
3. Z. Ungvari, S. Tarantini, A. J. Donato, V. Galvan, A. Csiszar, Mechanisms of vascular aging. *Circ. Res.* **123**, 849–867 (2018).
4. G. Cafueri *et al*., Endothelial and smooth muscle cells from abdominal aortic aneurysm have increased oxidative stress and telomere attrition. *PLoS One* **7**, e35312 (2012).
5. S. Liao, J. A. Curci, B. J. Kelley, G. A. Sicard, R. W. Thompson, Accelerated replicative senescence of medial smooth muscle cells derived from abdominal aortic aneurysms compared to the adjacent inferior mesenteric artery. *J. Surg. Res.* **92**, 85–95 (2000).
6. A. Watson *et al*., Nicotinamide phosphoribosyltransferase in smooth muscle cells maintains genome integrity, resists aortic medial degeneration, and is suppressed in human thoracic aortic aneurysm disease. *Circ. Res.* **120**, 1889–1902 (2017).
7. H.-Z. Chen *et al*., Age-associated sirtuin 1 reduction in vascular smooth muscle links vascular senescence and inflammation to abdominal aortic aneurysm. *Circ. Res.* **119**, 1076–1088 (2016).
8. D. H. Maurice *et al*., Advances in targeting cyclic nucleotide phosphodiesterases. *Nat. Rev. Drug Discov.* **13**, 290–314 (2014).
9. X. Qin *et al*., Smooth muscle-specific Gsα deletion exaggerates angiotensin II-induced abdominal aortic aneurysm formation in mice in vivo. *J. Mol. Cell. Cardiol.* **132**, 49–59 (2019).
10. D.-c. Guo *et al*.; GenTAC Registry Consortium; National Heart, Lung, and Blood Institute Grand Opportunity Exome Sequencing Project, Recurrent gain-of-function mutation in PRKG1 causes thoracic aortic aneurysms and acute aortic dissections. *Am. J. Hum. Genet.* **93**, 398–404 (2013).
11. Y. Cai *et al*., Role of cAMP-phosphodiesterase 1C signaling in regulating growth factor receptor stability, vascular smooth muscle cell growth, migration, and neointimal hyperplasia. *Circ. Res.* **116**, 1120–1132 (2015).
12. S. D. Rybalkin *et al*., Calmodulin-stimulated cyclic nucleotide phosphodiesterase (PDE1C) is induced in human arterial smooth muscle cells of the synthetic, proliferative phenotype. *J. Clin. Invest.* **100**, 2611–2621 (1997).
13. S. J. Netherton, D. H. Maurice, Vascular endothelial cell cyclic nucleotide phosphodiesterases and regulated cell migration: Implications in angiogenesis. *Mol. Pharmacol.* **67**, 263–272 (2005).
14. P. K. Bautista Niño *et al*., Phosphodiesterase 1 regulation is a key mechanism in vascular aging. *Clin. Sci. (Lond.)* **129**, 1061–1075 (2015).
15. A. Daugherty, L. A. Cassis, H. Lu, Complex pathologies of angiotensin II-induced abdominal aortic aneurysms. *J. Zhejiang Univ. Sci. B* **12**, 624–628 (2011).
16. K. Satoh *et al*., Cyclophilin A enhances vascular oxidative stress and the development of angiotensin II-induced aortic aneurysms. *Nat. Med.* **15**, 649–656 (2009).
17. G. Lu *et al*., A novel chronic advanced stage abdominal aortic aneurysm murine model. *J. Vasc. Surg.* **66**, 232–242.e4 (2017).
18. C. L. Miller *et al*., Role of Ca^{2+}/calmodulin-stimulated cyclic nucleotide phosphodiesterase 1 in mediating cardiomyocyte hypertrophy. *Circ. Res.* **105**, 956–964 (2009).
19. N. N. Hooten, M. K. Evans, Techniques to induce and quantify cellular Senescence. *J. Vis. Exp.* **123**, 55533 (2017).
20. L.-J. Min, M. Mogi, M. Iwai, M. Horiuchi, Signaling mechanisms of angiotensin II in regulating vascular senescence. *Ageing Res. Rev.* **8**, 113–121 (2009).
21. N. N. Deshpande *et al*., Mechanism of hydrogen peroxide-induced cell cycle arrest in vascular smooth muscle. *Antioxid. Redox Signal.* **4**, 845–854 (2002).
22. Y. Kida, M. S. Goligorsky, Sirtuins, cell senescence, and vascular aging. *Can. J. Cardiol.* **32**, 634–641 (2016).
23. Z. Wang *et al*., Cyclic AMP mimics the anti-ageing effects of calorie restriction by up-regulating sirtuin. *Sci. Rep.* **5**, 12012 (2015).
24. Z. Gerhart-Hines *et al*., The cAMP/PKA pathway rapidly activates SIRT1 to promote fatty acid oxidation independently of changes in NAD(+). *Mol. Cell* **44**, 851–863 (2011).
25. S. Xiong, G. Salazar, N. Patrushev, R. W. Alexander, FoxO1 mediates an autofeedback loop regulating SIRT1 expression. *J. Biol. Chem.* **286**, 5289–5299 (2011).
26. S.-C. Chao *et al*., Induction of sirtuin-1 signaling by resveratrol induces human chondrosarcoma cell apoptosis and exhibits antitumor activity. *Sci. Rep.* **7**, 3180 (2017).
27. D. J. Nagel *et al*., Role of nuclear Ca^{2+}/calmodulin-stimulated phosphodiesterase 1A in vascular smooth muscle cell growth and survival. *Circ. Res.* **98**, 777–784 (2006).
28. A. T. Bender, C. L. Ostenson, E. H. Wang, J. A. Beavo, Selective up-regulation of PDE1B2 upon monocyte-to-macrophage differentiation. *Proc. Natl. Acad. Sci. U.S.A.* **102**, 497–502 (2005).
29. R. Umebayashi *et al*., Cilostazol attenuates angiotensin II-induced abdominal aortic aneurysms but not atherosclerosis in apolipoprotein E-deficient mice. *Arterioscler. Thromb. Vasc. Biol.* **38**, 903–912 (2018).
30. Y. Liu *et al*., Inhibition of adenosine uptake and augmentation of ischemia-induced increase of interstitial adenosine by cilostazol, an agent to treat intermittent claudication. *J. Cardiovasc. Pharmacol.* **36**, 351–360 (2000).
31. S. Sartore *et al*., Contribution of adventitial fibroblasts to neointima formation and vascular remodeling: From innocent bystander to active participant. *Circ. Res.* **89**, 1111–1121 (2001).
32. M. Sata *et al*., Hematopoietic stem cells differentiate into vascular cells that participate in the pathogenesis of atherosclerosis. *Nat. Med.* **8**, 403–409 (2002).
33. B. C. Cooley *et al*., TGF-β signaling mediates endothelial-to-mesenchymal transition (EndMT) during vein graft remodeling. *Sci. Transl. Med.* **6**, 227ra34 (2014).
34. Y. Cai *et al*., Cyclic nucleotide phosphodiesterase 1 regulates lysosome-dependent type I collagen protein degradation in vascular smooth muscle cells. *Arterioscler. Thromb. Vasc. Biol.* **31**, 616–623 (2011).
35. Y. Yan *et al*., Dopamine controls systemic inflammation through inhibition of NLRP3 inflammasome. *Cell* **160**, 62–73 (2015).